Mechanical response of structural 3D printed polymers: an experimental and numerical study

Mechanical response of structural 3D printed polymers: an experimental and numerical study

Robin Delbart[1], Bence Toth[1], Francisca Martinez-Hergueta[1], Thuy Quynh Truong Hoang[2]
[1] School of Engineering, Institute for Infrastructures and Environment, University of Edinburgh, UK
[2] ESTACA Ecole d'ingénieurs, France

ABSTRACT

An experimental and numerical study on the mechanical response of 3D printed PLA components manufactured by Fused Deposition Modelling is presented. Special emphasis on the influence of layer height on the mechanical properties of printed coupons has been considered. Specimens were experimentally characterized under uniaxial tensile loads to determine the main deformation and failure mechanisms and understand the ratio between ultimate strength and equivalent density. Afterwards, the physical findings were used to develop a numerical model able to predict the mechanical response for different layer heights. Filaments were individually discretised and a cohesive zone model was used to capture interfilament debonding. Specimens exhibited an elasto-plastic response and the main failure mechanism was determined as filament debonding. The layer height played a significant role in the total volume of voids and the resultant mechanical properties, where it was found that the performance improved for small layer heights with an inherent porosity lower than 5%. In particular, a large dependency between porosity and homogenised macroscopic stiffness and strength was found. Nevertheless, porosity did not play a major role on the adhesion between filaments for the evaluated range. This document provides the basis to develop failure criteria for structural components manufactured by additive manufacturing.

1. INTRODUCTION

3D printing has evolved in recent years, showing great potential for multifunctional applications in aerospace, civil and bio-engineering sectors [1], however, the technology is not mature enough in terms of mechanical performance to create reliable components for primary structural applications [2]. Indeed, the different manufacturing methods available in 3D printing [3] have a poor fracture resistance hence current 3D printed devices are principally used for prototyping. Fused Deposition Modelling (FDM) is the most used technique in additive manufacturing, with a high versatility to print components based on thermoplastic polymers, synthetic, natural fibres, etc. One potential application is the in-situ printing of electric circuits in structural components using conductive PLA thermoplastic filaments.

Studies have been accomplished to determine the electronic properties of few different conductive filaments available on the market [4][5]. Mechanical properties of conventional 3D printed PLA have also been previously characterised by different authors [6], and it is possible to find in the literature the influence of different manufacturing parameters such as infill pattern, printing angle or layer height in the final stiffness and strength of the material [7]. However, there is currently a lack of numerical models that can predict the mechanical performance and failure of structural components based on 3D printed PLA. One of the main difficulties consists of modelling the complex inter-laminar and cross-laminar crack propagation of FDM components due to the low adhesion between adjacent filaments. It is possible to find preliminary studies modelling filament debonding by means of extended finite element method (XFEM), however, further research is required to understand the influence of manufacturing parameters such as layer height in the final inter-filament normal and shear strength of the material [8].

This study aims to develop a finite element model able to predict the mechanical response of 3D printed PLA components and capture their main failure mechanisms for different processing parameters. 3D printed samples with different layer height were manufactured and subjected to uniaxial tensile testing. Mechanical properties and failure modes have been compared against porosity to determine the optimal processing parameters to obtain lightweight components. Mechanical response improved when decreasing the layer height for very low levels of porosity. Based on these experimental findings, a numerical model was developed to understand the influence of manufacturing parameters in the final mechanical properties of the material. In this model, cohesive elements have been implemented to reproduce the debonding at the interface between each filament [9][10][11]. Good correlation in terms of stress-strain curves, strain to failure and crack propagation was obtained for different layer heights, and the differences in material parameters have been discussed.

2. MATERIAL & METHODS

2.1 Materials and manufacturing

For the present study, a commercial PLA filament with brand name Proto-Pasta supplied by the company Protoplant was selected. The filament is based on the Natureworks 4043 PLA polymer with a melt point of 155 ºC and contained a significant percentage of carbon black filler to increase the electrical conductivity. Dog bone specimens were designed according to the D6387 protocol, with an overall length of 165 mm, a gauge length of 57 mm, 13 mm in width and 3.2 mm thickness, see Fig.1. Specimens were manufactured by a Prusa i3 MK3S FDM printer. A hot-end temperature of 215 ºC and a printing bed temperature of 60 ºC was used as recommended by the manufacturer. The filament was extruded through a 0.4 mm diameter nozzle at 100% extrusion ratio. Filaments were laid down at ±45º with respect to the loading direction. Two perimeter layers were additionally included. Different layer heights of 0.05, 0.1 and 0.2 mm were selected to understand the influence of porosity in the final mechanical properties, resulting in equivalent weights of 9.08g, 9.73g and 10.42g respectively and a porosity (percentage of voids) of 4.4 %, 10.7 % and 16.7% respectively.

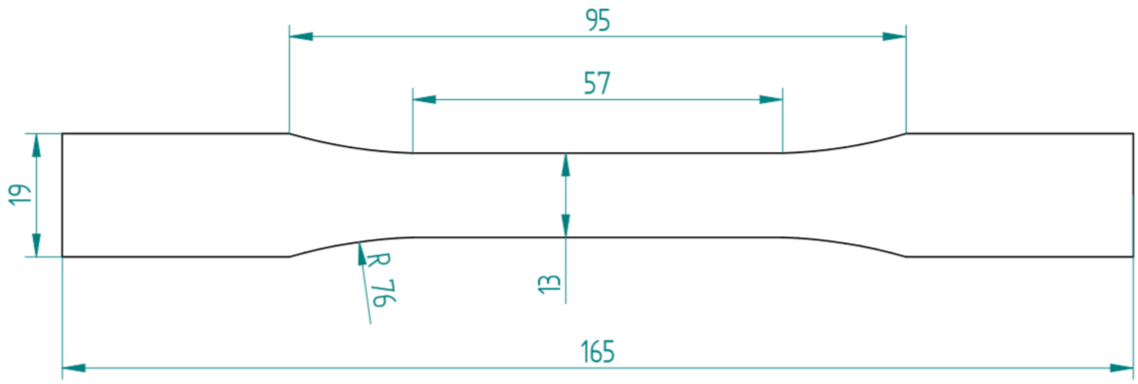

Figure 1. Dimensions of the coupons used for the mechanical characterisation.

2.2 Mechanical testing

Quasi-static tests were accomplished with the actuator of a MTS Criterion® Series 4 screw-driven testing frame. Tensile tests were carried out following the ASTM D638 standard under stroke control at cross head speed of 5 mm/min. The load was recorded continuously with a 300 kN load cell together with the cross-head displacement of the testing frame. Additionally, in-situ Digital Image Correlation (DIC) was used to acquire the longitudinal displacement of the gauge section during the mechanical tests. The black polymer specimens were speckled with white paint to capture the local strain field. Full field displacement measurements in the specimen were carried out using an Imetrum uvx camera at 5 fps and 1392 x 1038 pixels resolution. Analysis was performed with the software GOM-Correlate. Window size and distance were selected to provide 1700 tracking points per image. 5 specimens were tested per layer height, force and strain data were processed in Matlab to obtain Young's modulus, Poisson's ratio, ultimate strength, and elongation at break of every sample.

3. MODELLING

Numerical simulation of the mechanical response of the 3D printed coupons were performed to get a better understanding of the deformation and fracture mechanisms upon uniaxial stretching. Simulations were carried out using the Finite Element Method (FEM) in Abaqus/Implicit. The FEM included the gauge section of the tensile specimens and discretised the filaments individually to reproduce interfilament failure. Elasto-plastic behaviour of the PLA polymer was implemented by a standard isotropic yielding model. The Mises yield surface was defined by the relationship between the uniaxial yield stress, σ, as function of uniaxial equivalent plastic strain, ε_{pl}, given by the following potential relationship:

$$\sigma = h\varepsilon_{pl}^{n}$$

where h and n are the material hardening coefficients. The elastic Young's Modulus, E, and the Poisson's ratio, were also defined to compute the recoverable strains, see the material parameters in Table 1. Values on this table were directly obtained from the experimental campaign explained in previous *Section 2.*

Table 1. Material properties of the 3D PLA as function of the layer height.

Layer height **(mm)**	***0.2***	***0.05***
Young's Modulus, E, (GPa)	1.70	2.47
Poisson's ratio, ν	0.32	0.33
Hardening coefficient, h (GPa)	0.412	0.781
Hardening exponential, n	0.725	0.803

Interfilament debonding was replicated by means of a classical cohesive zone method using cohesive elements whose behaviour was dictated by a traction-separation law. A stress-based damage initiation was considered following a quadratic interaction criterion between normal and shear stresses on the interface:

$$\left(\frac{< t_n >}{N}\right)^2 + \left(\frac{t_s}{S}\right)^2 + \left(\frac{t_t}{S}\right)^2 = 1$$

where t_n, t_s, and t_t were the normal shear elastic stresses acting on the interface and N and S stand for the normal and shear interface strengths, respectively. Once the stress failure criterion was fulfilled, the damage evolves depending on the interply toughness of the interface according to the Benzeggah-Kenane fracture criterion.

$$\Gamma_C = \Gamma_{Ic} + (\Gamma_{IIc} - \Gamma_{Ic})\left(\frac{\Gamma_s + \Gamma_t}{\Gamma_n + \Gamma_s + \Gamma_t}\right)^{\eta}$$

where Γ_{Ic} and Γ_{IIc} are the critical energy release rates for delamination in modes *I* and *II* respectively, assuming $\Gamma_{IIc} = \Gamma_{IIIc}$. Γ_s, Γ_n, Γ_t were the work done by the tractions and their conjugate relative displacements in the normal and shear directions and η corresponded to the parameter that determined the increase in toughness with the amount of mode mixity. Interface properties were independent from the layer height and are included in Table 2. Notice the large value of the defined fracture toughnesses to reproduce the ductility of the filament interface.

Table 2. Interfilament properties.

Material properties	**Value**
Normal interface strength, *N,* (MPa)	100
Shear interface strength, *S,* (MPa)	100
Mode I fracture toughness, Γ_{Ic}, (N/mm)	100
Mode II fracture toughness, Γ_{IIc}, (N/mm)	100
Benzeggagh-Kenane parameter, η	1.75

Single layers of the 3D printed coupons were discretised at filament level with 8 nodes reduced integration linear solid elements (C3D8R) inserting three-dimensional cohesive elements (COH3D8) with 0.001 mm thickness between filaments to account for debonding. Layers had a variable height (0.2 and 0.05 mm) and fixed width of 0.4 mm corresponding to the nozzle diameter, see Fig. 2. The mesh was aligned towards the deposition trajectory and final number of elements was 18836. Quasi-static tests were simulated clamping one of the edges of the specimen and imposing a displacement of 3 mm to the opposite boundary. It should be noted that the default bulk viscosity option in Abaqus was used in the simulations to eliminate instabilities in the numerical model at the onset of damage. Simulations had a computational cost of approximately 1 hour.

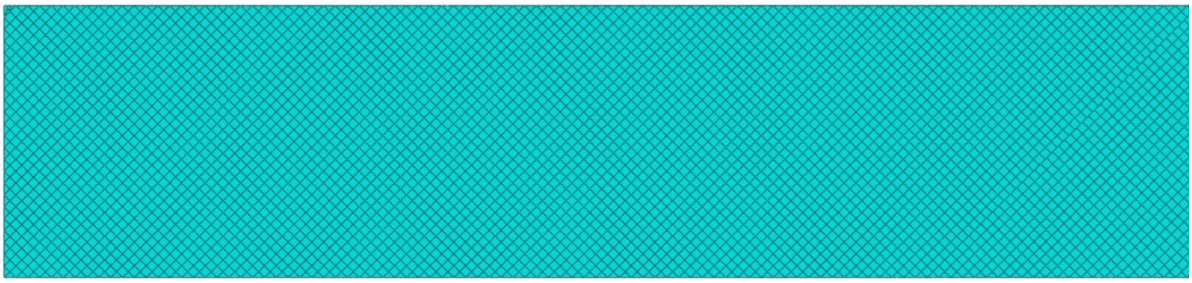

Figure 2. Example of the finite element discretisation technique used in the FEM.

4. RESULTS AND DISCUSSION

The uniaxial tensile response of the 3D printed specimens was characterised and representative nominal stress *vs.* engineering strain curves are plotted in Fig. 3 (a) for three different layer heights. The average values of equivalent porosity, the Young's Modulus, ultimate strength and elongation at break are depicted in Table 3, together with the standard deviation. All configurations showed a non-linear elasto-plastic response, however, stiffness, strength and strain to failure differed among layer heights.

The stiffness and the ultimate strength of the printed coupons increased when decreasing the layer height, however, significant improvement was exhibited for the lower layer height of 0.05 mm, with final properties equivalent to the stiffness and strength of bulk semicrystalline PLA polymer [12]. Good repeatability of the Poisson's ratio (around 0.34) was obtained, however, large scattering in the final strain to failure was found ranging from 2.0 to 6.5%, although higher repeatability was obtained when decreasing the layer height. As the layer height decreased, the equivalent density of the specimens increased, resulting in a lower porosity and volume of voids inside the sample. Fig 3(b) plots the ratio between the strength and the weight of the samples *vs* the equivalent porosity. The 3D printed PLA components exhibited a linear relationship between strength and equivalent density for porosity levels higher than the 10%, nevertheless significant improvements were obtained in specific terms when decreasing the porosity of the specimens up to 5%. It should be noted that those levels of low porosity can be only achieved when using fine nozzles and longer printing times, with a resultant cost increment of the manufacturing process. Further research at lower layer printing height can provide further insight in the relationship between mechanical properties and manufacturing cost.

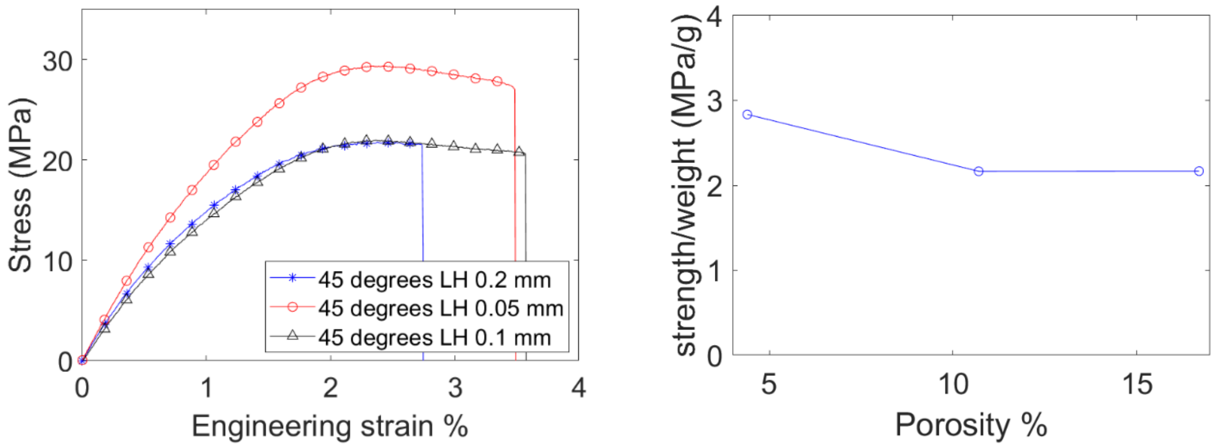

Fig. 3. Tensile response of the 3D printed PLA coupons. (a) Representative engineering stress *vs.* engineering strain curves for the different layer heights. (b) Ratio between the ultimate strength and the sample weight *vs.* porosity (% of voids).

Failure mechanisms were analysed by DIC and the evolution of the full-field engineering strain along the loading axis for a coupon of 0.05 mm layer height is shown in Fig. 4. The specimens presented a homogeneous strain field before damage localisation, where cracks developed following the printing direction; at ±45° in the central region and perpendicular to the loading direction in the periphery of the specimen. This resulted in two distinctive failure modes: filament debonding and filament tensile failure. Onset of damage was usually registered from the central regions of the specimens where the misalignment between filaments initially occurred and extend to the edge of the specimen.

Table 3. In-plane tensile mechanical properties of the PLA coupons as function of the layer height.

Layer Height (mm)	Porosity (%)	Young Modulus (GPa)	Maximal Stress (MPa)	Elongation at break
0.2	16.7 ± 0.1	1.70 ± 0.09	19.68 ± 1.24	0.04 ± 0.02
0.1	10.7 ± 0.1	1.72 ± 0.11	21.07 ± 0.59	0.050 ± 0.015
0.05	4.4 ± 0.1	2.47 ± 0.05	29.54 ± 0.26	0.040 ± 0.007

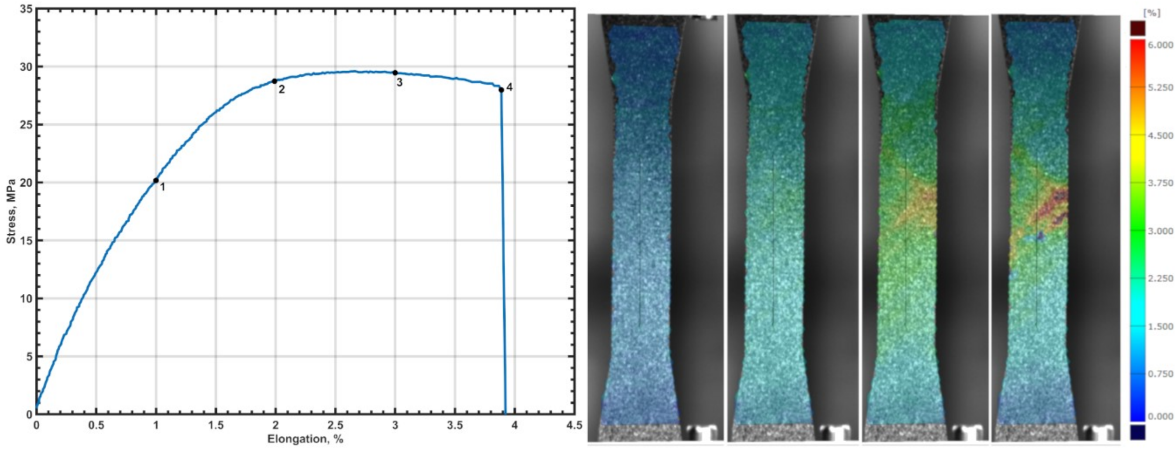

Fig. 4. Evolution of local strain during uniaxial deformation ε_{11}. (a) Representative engineering stress *vs.* engineering strain curve for a specimen with 0.05 mm layer height and correspondent contour plots of the engineering longitudinal strain at (b) 1%, (c) 2%, (d) 3% deformation and (e) strain to failure.

Prediction of the mechanical response obtained by FEM was in good agreement with the experimental results in terms of stiffness and ultimate strength for the different layer heights. Fig. 5 shows the correlation between experimental and numerical stress-strain curves. The main difference was identified after onset of damage. The numerical model captured accurately the elasto-plastic response of the polymer and the onset of damage at around 2% of deformation for both layer heights, within the experimental range. Strain gradients were also in good correlation to DIC observations. Fig. 6 compares the longitudinal strains at different elongation levels before and after onset of damage for 0.05 layer height. The numerical simulation captured the homogeneous deformation of the specimens before the onset of damage (2% of deformation) as well as the damage localisation and filament debonding.

At the maximum loading capacity of the material, filament debonding was triggered by the cohesive elements. Although the damage initiation criteria accurately captured the onset of damage, further work is required to understand damage evolution of inter-filament interfaces and 3D printed materials. Despite the experimental fracture surface clearly identifying the main failure mechanisms as filament debonding, the obtained stress-strain curve is representative of bulk polymers subjected to uniaxial tensile loads undergoing yielding and necking due to localised plastic deformation [12]. Cohesive elements can effectively reproduce brittle failure modes, for example, delamination of composite materials, however, further analysis of energy release rates need to be accomplished to develop robust constitutive models able to replicate the ductility experienced by 3D printed PLA components.

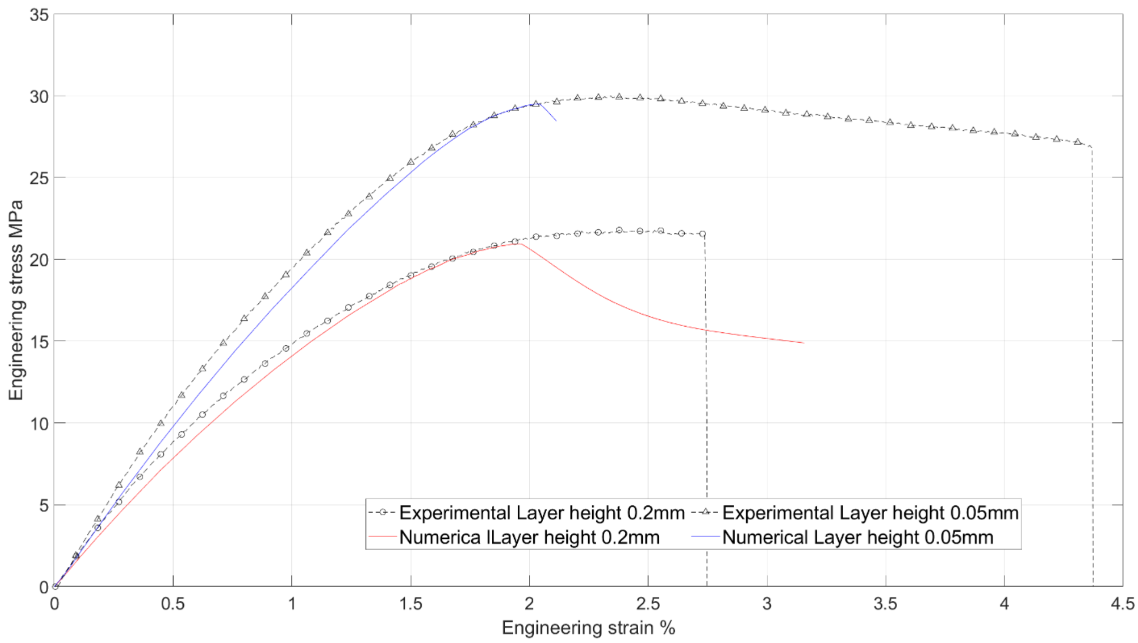

Fig. 5. Comparison between the numerical and experimental result of the Engineering stress vs Engineering strain of the 0.05 mm and 0.2 mm layer height samples.

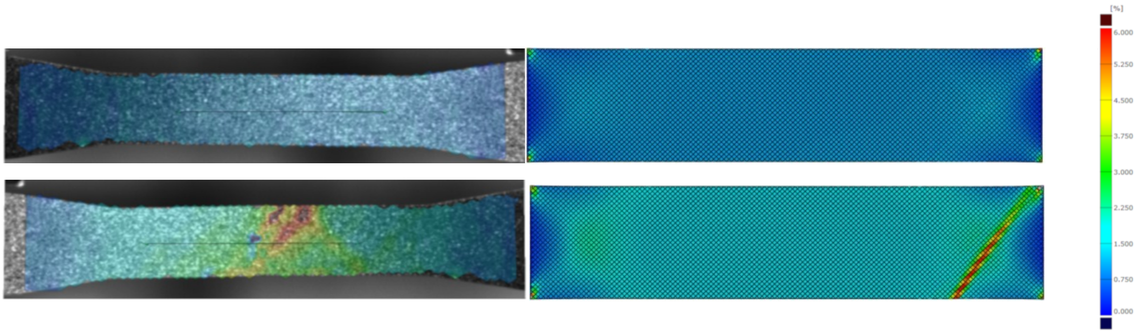

Fig. 6. Experimental and numerical contour of the longitudinal strain ε_{11} at 1% (top images) and when the crack happening (bottom images) on the 0.05 mm ±45º sample

The mechanical response of 3D printed components with different porosity levels were introduced, tailoring the stress-strain curve of the elasto-plastic PLA filament, see Table 1. Nonetheless, it should be noted that the material parameters defining the quadratic damage criterion of the cohesive elements used to capture the interfilament debonding were identical for all the simulations, see Table 2. Considering these results, it can be stated that chemical adhesion between filaments was similar for all the tested configurations and remained independent on parameters such as deposition velocity and porosity for the given geometry. Mechanical performance of the printed PLA filament was driven by the volume of voids, however, the non-linear relationship between strength and apparent density for low porosity levels indicated a complex interaction between voids and failure mechanisms at lower scales. The role of porosity in the final stiffness of the material needs to be further explored to improve the mechanical performance of the 3D printed polymers, and the influence of microstructural parameters such as void size, distribution and topology should to be analysed by micromechanical in-situ testing, to develop physically-based failure criteria for stress analysis.

5. CONCLUSIONS

A numerical model was developed to replicate the mechanical response of 3D printed PLA coupons subjected to uniaxial tensile loads. The role of different processing parameters such as layer height in the final stiffness and strength of the material were evaluated. The experimental elasto-plastic tensile response of the material was driven by the volume of voids, with a remarkable increment of specific stiffness and ultimate strength when decreasing the level of porosity to values lower than 5%. The main failure mechanism was ascertained as interfilament debonding, with negligible influence of tensile filament failure. The physical findings were used to develop a numerical model able to account for the complex failure mechanisms. Filaments were individually discretised and interfilament debonding was reproduced by cohesive elements. Differences between layer height were accounted by the material elasto-plastic properties of the PLA filament, however, material parameters of the cohesive elements were maintained identical for all configurations. Good agreement in terms of stiffness, strength and failure modes was found between experiments and simulations. This study demonstrated the ability of the cohesive zone model approach to reproduce the catastrophic failure of 3D printed devices, especially those manufactured by fused deposition modelling. Despite adhesion between filaments remaining similar within the analysed porosity range, significant differences were exhibited in the stiffness and strength of the material at the homogeneous macroscale. Complex interaction between voids and failure mechanisms can be perceived, and further studies at a lower microscale will provide robust insight to develop future failure criteria for 3D printed structural components.

6. ACKNOWLEDGEMENTS

This investigation was supported by the Defence Science and Technology Laboratory (DSTL) of the Ministry of Defence of UK through the grant [DSTLX1000144021R].

7. REFERENCES

[1] Wang, Xin, et al. "3D printing of polymer matrix composites: A review and prospective." Composites Part B: Engineering 110 (2017): 442-458.

[2] Z. Tong, «Additive manufacturing for micro-architecture: A mini review».

[3] Ngo, Tuan D., et al. "Additive manufacturing (3D printing): A review of materials, methods, applications and challenges." Composites Part B: Engineering 143 (2018): 172-196.

[4] Kwok, Sen Wai, et al. "Electrically conductive filament for 3D-printed circuits and sensors." Applied Materials Today 9 (2017): 167-175.

[5] Gnanasekaran, Karthikeyan, et al. "3D printing of CNT-and graphene-based conductive polymer nanocomposites by fused deposition modeling." Applied materials today 9 (2017): 21-28.

[6] Song, Yichi, et al. "Measurements of the mechanical response of unidirectional 3D-printed PLA." *Materials & Design* 123 (2017): 154-164.

[7] Fernandez-Vicente, Miguel, et al. "Effect of infill parameters on tensile mechanical behavior in desktop 3D printing." 3D printing and additive manufacturing 3.3 (2016): 183-192.[8] Ghandriz, R., K. Hart, and J. Li. "Extended finite element method (XFEM) modeling of fracture in additively manufactured polymers." Additive Manufacturing 31 (2020): 100945.

[8] Chacón, J. M., et al. "Additive manufacturing of PLA structures using fused deposition modelling: Effect of process parameters on mechanical properties and their optimal selection." Materials & Design 124 (2017): 143-157.

[9] Huzni, S., et al. "Finite element modeling of delamination process on composite laminate using cohesive elements." International Journal of Automotive and Mechanical Engineering 7 (2013): 1023.

[10] Martínez-Hergueta, F., et al. "Modelling the in-plane strain rate dependent behaviour of woven composites with special emphasis on the non-linear shear response." Composite Structures 210 (2019): 840-857.

[11] LLorca, Javier, et al. "Multiscale modeling of composite materials: a roadmap towards virtual testing." Advanced Materials 23.44 (2011): 5130-5147.

[12] Yang, Sen-lin, et al. "Thermal and mechanical properties of chemical crosslinked polylactide (PLA)." Polymer Testing 27.8 (2008): 957-963.